LETTERS
PUBLISHED ONLINE: 27 MAY 2012 | DOI: 10.1038/NMAT3333
nature materials

High intergrain critical current density in fine-grain $(Ba_{0.6}K_{0.4})Fe_2As_2$ wires and bulks

J. D. Weiss, C. Tarantini, J. Jiang, F. Kametani, A. A. Polyanskii, D. C. Larbalestier and E. E. Hellstrom*

The K- and Co-doped $BaFe_2As_2$ (Ba-122) superconducting compounds are potentially useful for applications because they have upper critical fields (H_{c2}) of well over 50 T, H_{c2} anisotropy $\gamma < 2$ and thin-film critical current densities J_c exceeding 1 MA cm^{-2} (refs 1–4) at 4.2 K. However, thin-film bicrystals of Co-doped Ba-122 clearly exhibit weak link behaviour for [001] tilt misorientations of more than about 5°, suggesting that textured substrates would be needed for applications, as in the cuprates[5,6]. Here we present a contrary and very much more positive result in which untextured polycrystalline $(Ba_{0.6}K_{0.4})Fe_2As_2$ bulks and round wires with high grain boundary density have transport critical current densities well over 0.1 MA cm^{-2} (self-field, 4.2 K), more than 10 times higher than that of any other round untextured ferropnictide wire and 4–5 times higher than the best textured flat wire[7]. The enhanced grain connectivity is ascribed to their much improved phase purity and to the enhanced vortex stiffness of this low-anisotropy compound ($\gamma \sim 1$–2) when compared with $YBa_2Cu_3O_{7-x}$ ($\gamma \sim 5$).

The tendency of grain boundaries (GBs) of the high-temperature superconducting cuprates such as $YBa_2Cu_3O_{7-x}$ to be weak linked has been the main impediment to producing wires needed for their application[8,9]. In the search for new classes of superconductors that might displace Nb–Ti and Nb_3Sn, the new Fe-based superconductors also demand attention, even though they seem to share similar non-superconducting parent phases to each other and have low carrier densities[10]. Bulk ferropnictide materials made thus far exhibit low global J_c (J_c^{global}) values, some of which can be ascribed to extrinsic factors such as their less than full density, the prevalence of GB-wetting phases, and cracking[11–16]. As a result, J_c^{global} of randomly oriented ferropnictide wires are typically well below 0.01 MA cm^{-2} (refs 11,17,18), although a recent textured K-doped $SrFe_2As_2$ (Sr-122; ref. 7) tape reports about 0.025 MA cm^{-2} at self-field. These values are one to two orders of magnitude less than the local intragrain critical current density J_c^{local} measured in single crystals[19–21]. A potentially serious intrinsic problem is the weak link behaviour of GBs in $Ba(Fe_{1-x}Co_x)_2As_2$ similar to that observed in the cuprates $YBa_2Cu_3O_{7-x}$ (YBCO) and $Bi_2Sr_2CaCu_2O_8$ (Bi-2212). However, the intergrain critical current density across [001] tilt misoriented GBs (J_c^{GB}) decreases less rapidly with increasing grain misorientation angle than in YBCO (refs 5,6,10). The generality of this result is still unclear though because thin-film bicrystals of ferropnictides have so far been grown for one structure (Ba-122) in only the Co-doped variant owing to the difficulty of maintaining proper composition control during deposition. Therefore, the study of polycrystalline samples is still of great importance. Here we report a surprisingly positive result with $(Ba_{0.6}K_{0.4})Fe_2As_2$ bulks and wires made by careful low-temperature synthesis showing much higher J_c^{global} than in Co-doped Ba-122 bulks. The very fine grain size (~200 nm), which is comparable to or smaller than the penetration depth, and the low H_{c2} anisotropy provide a basis for high vortex stiffness. The enhanced phase purity at the GBs and low anisotropy seem to enable transport critical current densities that are high enough to be interesting for applications.

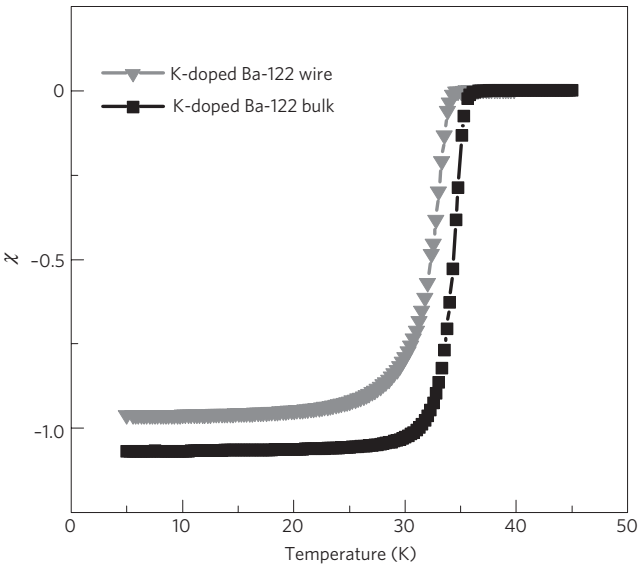

Figure 1 | Volumetric magnetic susceptibility as a function of temperature for K-doped Ba-122 wire and bulk. The magnetic response was evaluated by warming above T_c after zero-field-cooling to 5 K and applying a field of 2 mT parallel to the sample's length.

K-doped Ba-122 polycrystals were fabricated by a reaction pathway that results in a more complete reaction, minimizing the formation of current-blocking secondary phases, such as FeAs, that tend to wet the GBs when higher temperatures are used. Keeping the reaction temperature well below the melting temperature of Fe–As phases ensures that the impurities present do not wet GBs where they would severely block the flow of supercurrent. Another benefit of low-temperature reactions is that the grain size of the Ba-122 phase is very fine, ~200 nm. Moreover, the bulk forms were easily powdered and made into a wire by the powder-in-tube technique, and short lengths of these wires were reacted and characterized. Details of our reaction process are in the Methods.

Applied Superconductivity Center, National High Magnetic Field Laboratory, Florida State University, Tallahassee, Florida 32310, USA.
*e-mail: Hellstrom@asc.magnet.fsu.edu.

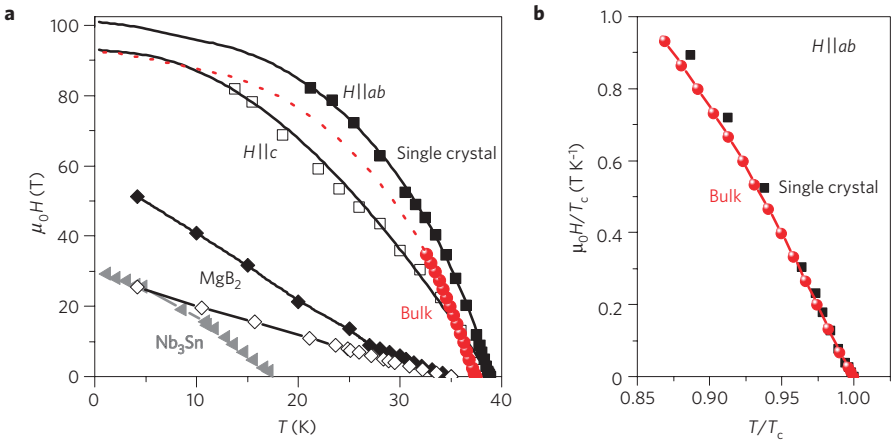

Figure 2 | Upper critical field as a function of temperature. a, H_{c2}(T) defined as 90% of the normal-state resistance for the K-doped Ba-122 bulk compared with an optimally doped single crystal from ref. 4, a Nb_3Sn wire from ref. 22 and a textured MgB_2 thin film from ref. 23 with H applied parallel (filled symbols) and orthogonal (open symbols) to its surface. The dotted line is a rescaled fit from ref. 4 to guide the eye. **b**, H_{c2} and temperature normalized by T_c to show close agreement between bulk polycrystal and single crystal samples with $H||ab$.

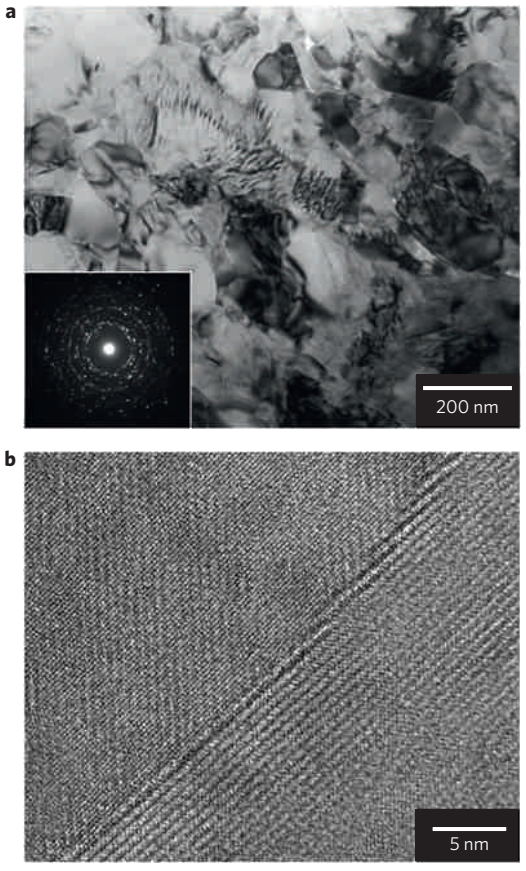

Figure 3 | Microstructures of K-doped Ba-122 bulk investigated by TEM imaging. a, TEM image of polycrystalline bulk K-doped Ba-122 material showing several equiaxed grains with average grain diameter of ~200 nm. Inset: A selected-area electron diffraction image of **a** that indicates that the grains of the material are randomly oriented with many high-angle GBs. **b**, HRTEM image of a typical K-doped Ba-122 GB where the TEM sample was tilted so the electron beam was almost parallel to the GB plane. The lattice fringes of upper and bottom grains meet at the GB without an amorphous contrast, indicating that the GB is clean without a wetting impurity phase.

Careful studies of electromagnetic granularity and the broader superconducting properties were made by superconducting quantum interference device magnetometry for critical temperature (T_c), vibrating sample magnetometry to measure the global magnetic moment in high fields, magneto-optical imaging to measure local granularity on scales of a few micrometres, and transport critical current measurements to determine the global transport current densities. Microstructures were examined at multiple length scales in a Zeiss 1540 EsB/XB scanning electron microscope (SEM) and a JEOL JEM2011 transmission electron microscope (TEM) to assess the size and distribution of secondary phases, the prevalence of cracking and the grain size of the Ba-122 phase.

Figure 1 shows the magnetic T_c transition of both wire and bulk in a magnetic field of 2 mT. Both samples show a strong diamagnetic signal with little temperature dependence corresponding to superconducting volume fraction >90%, indicating strong global screening currents crossing many high-angle GBs. To characterize H_{c2}(T), the bulk resistance was measured by a 4-point method in magnetic fields up to 35 T. The resistivity measurements can be found in Supplementary Fig. S1. As seen in Fig. 2a, $H_{c2}(0)$ is estimated above 90 T for K-doped Ba-122, well beyond the highest values obtained for Nb_3Sn (ref. 22) wires and MgB_2 (ref. 23) thin films and comparable to the K-doped Ba-122 single crystal[4] plotted for comparison. Figure 2b shows the bulk and single crystal ($H||ab$) data[4] normalized by their respective T_c (bulk: 37.4 K, crystal: 38.7 K). The excellent agreement with single crystal data also confirms that this bulk polycrystal is of high quality because H_{c2} of this compound has been shown to be very sensitive to doping[4].

Figure 3 shows a TEM image of the polycrystalline K-doped bulk. The diffraction contrast in Fig. 3a clearly shows that the average grain size is approximately 200 nm. The electron diffraction pattern from the selected area of Fig. 3a indicates a randomly oriented polycrystalline structure containing many high-angle GBs. The high-resolution TEM observation confirms clean and well-connected GBs in a randomly oriented polycrystalline bulk, as shown by a typical GB in Fig. 3b. However, TEM images do reveal some porosity and secondary phase that obstruct some current flow, indicating room for further process optimization. The impurity phase was identified by X-ray diffraction as FeAs and accounts for less than 3% of the bulk volume by SEM image analysis (see Supplementary Figs S2 and S3). Supplementary Fig. S4 shows TEM images and the electron diffraction pattern

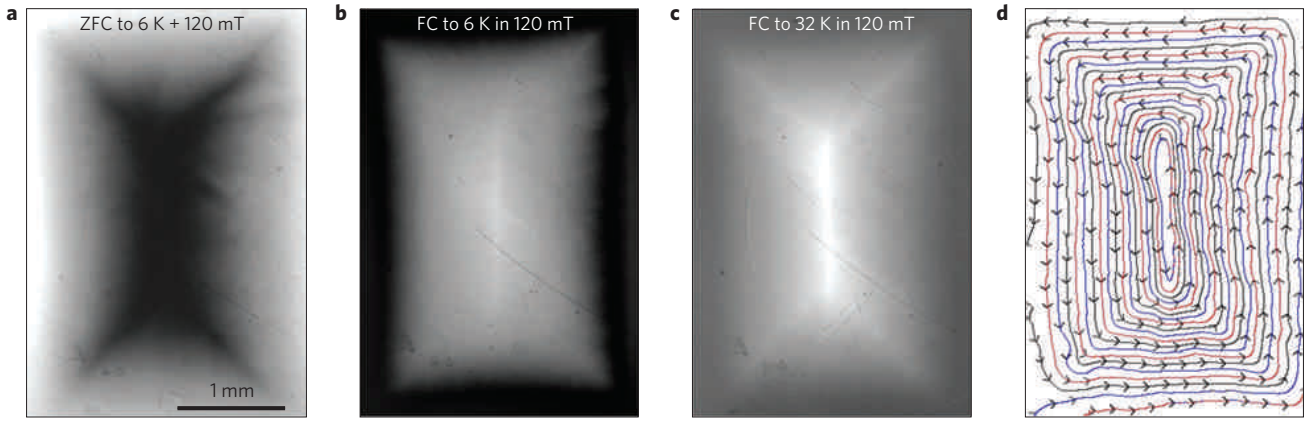

Figure 4 | Magneto-optical images of a rectangular piece of K-doped Ba-122 bulk material with magnetic fields applied perpendicular to the plane of the sample (thickness = 0.7 mm). a, Magneto-optical image of partial flux penetration after zero-field-cooling (ZFC) the sample to 6 K and applying a magnetic field of 120 mT. **b**, Magneto-optical image of trapped magnetic flux in a sample field-cooled (FC) to 6 K in an external magnetic field of 120 mT. **c**, Magneto-optical image of trapped magnetic flux in a sample field-cooled to 32 K in an external magnetic field of 120 mT. **d**, Current stream lines calculated for **c** that illustrate the uniform current distribution that circulates inside the bulk even near T_c.

of Co-doped Ba-122 material that has a microstructure similar to the K-doped 122. Magneto-optical imaging was used to image the local field profile B_x produced by magnetization currents induced by magnetic fields of up to 120 mT applied perpendicular to the bulk sample's surface. The magneto-optical images in Fig. 4 show a rooftop pattern of magnetic flux density produced by bulk current flow over the entire ~3-mm-long sample, a length scale that is orders of magnitude larger than the ~200 nm grain size seen in Fig. 3a. Figure 4a shows only a partial flux penetration due to strong induced currents caused by applying a magnetic field of 120 mT after zero-field-cooling the sample to 6 K. Figure 4b and c show uniform, fully trapped, magnetic flux from applying a magnetic field of 120 mT and then field-cooling the sample from above T_c to 6 K and 32 K, respectively. The calculated current stream lines for the 32 K field-cooled magneto-optical image in Fig. 4c are shown in Fig. 4d. Very uniform bulk current flow is still present above 30 K, a testament to the material's electromagnetic homogeneity and large superconducting volume fraction even close to T_c. Magneto-optical images of a cross-section of our K-doped wire (Supplementary Fig. S5) also show good electromagnetic homogeneity comparable to the bulk material. In contrast, magneto-optical images of other ferropnictide bulks show primarily granular currents indicating little or no bulk current flow[1,15]. Clearly, magneto-optical imaging indicates there is significant and well distributed J_c^{global} in our material.

Figure 5 shows $J_c^{magnetization}$ and $J_c^{transport}$ of the wire plotted as a function of applied magnetic fields along with other round untextured Fe-based superconducting wires[13,24]. $J_c^{transport}$, measured for H perpendicular to the wire's length, was calculated from the critical current (I_c) using the area of the superconducting cross-section of the wire (see Fig. 5 inset). I_c was determined using the electric field criterion $E_c = 1\,\mu V cm^{-1}$ (see Supplementary Fig. S6 for current–voltage curves). $J_c^{magnetization}$ was calculated from vibrating sample magnetometry measurements using the Bean model. The good agreement between the transport and magnetization measurements indicates the intragrain J_c^{local} component makes only a small contribution to the magnetization. At self-field, a high J_c^{global} of over 0.12 MA cm^{-2} is obtained, the highest reported J_c^{global} of any ferropnictide bulk or wire so far. J_c^{global} shows a weak field dependence and maintains a reasonably high value of 0.01 MA cm^{-2} at 12 T. This is over an order of magnitude higher than the best untextured wires and about three times higher than the textured Sr-122 tape reported in ref. 7 at 10 T. Not only are these values

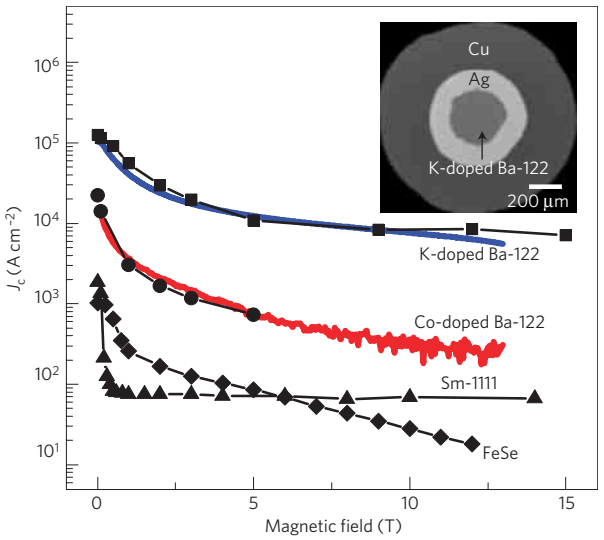

Figure 5 | $J_c^{transport}$ and $J_c^{magnetization}$ as a function of applied magnetic field at 4.2 K for the K-doped wire, compared with other round, untextured, Fe-based superconducting wires. Symbols, $J_c^{transport}$; solid lines, $J_c^{magnetization}$. Sm-1111 wire is from ref. 13 and FeSe wire is from ref. 24. Inset: SEM image of the K-doped mono-core wire showing the round cross-section with Ag and Cu sheaths.

high for ferropnictide materials, but they approach the J_c^{global} values desired for applications.

An SEM image of the cross-section of the K-doped Ba-122 wire is shown in the inset in Fig. 5. The round wires made by powder-in-tube processing are advantageous because they can be made cheaply and applied to traditional designs that depend on electromagnetically isotropic round wires. As the superconductor is made *ex situ* and the final heat treatment is short and does not exceed 600 °C, sheath materials other than Ag may also be used without significantly degrading the conductor owing to chemical reactions that occur with the sheath material at high temperatures. This may allow for the use of stronger, less expensive sheath materials. We have yet to explore in detail the effect of texturing, adding other dopants, multi-core wires or over-doping potassium, all of which have been shown to increase J_c in ferropnictide wires or tapes[7,12,25,26].

We propose that the unexpectedly high J_c^{global} arises through a combination of factors. First, our heat treatment occurs at a

sufficiently low temperature that secondary phases do not wet GBs, as earlier studies showed that such phases block current[16]. Second, high-pressure synthesis results in nearly 100% dense material, which further contributes to good connectivity. Third, the fine grain size makes planar GBs very rare and the low γ value makes the vortex stiffness high. Thus, although essentially all vortices cross GBs, which may have a depressed superconducting order parameter, the GB vortex portion is short and can be anchored by the strong pinning of the superconducting segments lying in the grains. This situation has been studied for YBCO bicrystals with planar GBs by varying the angle between the magnetic field and the GB plane[10,27]. Only when the two are close and a significant length of vortex lies in the GB is the GB J_c depressed below the intragrain J_c value. In our K-doped Ba-122 bulks and wires, which have very small grains and thus a high density of non-planar GBs plus a small γ, we may expect that very little of the vortices actually lies in any GB. A final possibility is that the K-doped compound may have less depressed GB order parameters, perhaps due to a higher carrier density induced by K segregation to the GBs. The higher J_c^{global} of the K-doped wire when compared with the Co-doped wire plotted in Fig. 5 suggests that particular compound-related factors may also be playing a role, whether due to differences in GB properties[28] or to the role of hole (K), rather than electron (Co) doping in Ba-122. Bicrystal experiments on the K-doped Ba-122 will be valuable to explore the specific properties of planar GBs that are possibly less weak linked than in other superconductors.

Methods

The elements were first mixed to obtain nominal composition $(Ba_{0.6}K_{0.4})Fe_2As_2$ or $Ba(Fe_{0.92}Co_{0.08})_2As_2$ and then ball milled for 1 h. During the milling, an exothermic reaction occurred, partially reacting the material to the Ba-122 phase. The ball-milled material was wrapped with Nb foil and placed in a stainless-steel ampoule that was evacuated, welded shut, compressed into a pellet with a cold isostatic press at 275 MPa, and then heat treated in a hot isostatic press under 192 MPa of pressure at 600 °C for 20 h. The material was re-milled and heat treated again as above for 10 h to obtain a more homogeneous bulk. For the wires, the bulk material was milled after the previous two steps and packed into a Ag tube (6.35 mm outer diameter, 4.35 mm inner diameter). The tube ends were plugged, swaged and welded shut. The tube was then groove rolled, followed by drawing to a 0.8-mm-outer-diameter wire. Pieces of the Ag-clad wire were sealed in Cu tubing (1.57 mm outer diameter, 0.86 mm inner diameter) under vacuum by welding the ends shut. The Cu tubing was then groove rolled to an outer diameter of ~1.35 mm. The Cu/Ag-clad wires were then compressed in a cold isostatic press under 2 GPa pressure and heat treated for 10 h at 600 °C in the hot isostatic press, as above.

Received 12 January 2012; accepted 17 April 2012; published online 27 May 2012

References

1. Putti, M. *et al.* New Fe-based superconductors: Properties relevant for applications. *Supercond. Sci. Technol.* **23,** 034003 (2010).
2. Lee, S. *et al.* Template engineering of Co-doped $BaFe_2As_2$ single-crystal thin films. *Nature Mater.* **9,** 397–402 (2010).
3. Katase, T. *et al.* Biaxially textured cobalt-doped $BaFe_2As_2$ films with high critical current density over 1 MA/cm^2 on MgO-buffered metal-tape flexible substrates. *Appl. Phys. Lett.* **98,** 242510 (2011).
4. Tarantini, C. *et al.* Significant enhancement of upper critical fields by doping and strain in iron-based superconductors. *Phys. Rev. B* **84,** 184522 (2011).
5. Lee, S. *et al.* Weak-link behavior of grain boundaries in superconducting $Ba(Fe_{1-x}Co_x)_2As_2$ bicrystals. *Appl. Phys. Lett.* **95,** 212505 (2009).
6. Katase, T. *et al.* Advantageous grain boundaries in iron pnictide superconductors. *Nature Commun.* **2,** 409 (2011).
7. Gao, Z. *et al.* High transport critical current densities in textured Fe-sheathed $Sr_{1-x}K_xFe_2As_2$ + Sn superconducting tapes. *Appl. Phys. Lett.* **99,** 242506 (2011).
8. Hilgenkamp, H. & Mannhart, J. Grain boundaries in high-T_c superconductors. *Rev. Mod. Phys.* **74,** 485–549 (2002).
9. Larbalestier, D. C., Gurevich, A., Feldmann, D. M. & Polyanskii, A. A. High-T_c superconducting materials for electric power applications. *Nature* **414,** 368–377 (2001).
10. Durrell, J. H. *et al.* The behavior of grain boundaries in the Fe-based superconductors. *Rep. Prog. Phys.* **74,** 124511 (2011).
11. Ma, Y. *et al.* Fabrication and characterization of iron pnictide wires and bulk materials through the powder-in-tube method. *Physica C* **469,** 651–656 (2009).
12. Wang, L. *et al.* Large transport critical currents of powder-in-tube $Sr_{0.6}K_{0.4}Fe_2As_2$/Ag superconducting wires and tapes. *Physica C* **470,** 183–186 (2010).
13. Wang, L. *et al.* Low-temperature synthesis of $SmFeAsO_{0.7}F_{0.3-\delta}$ wires with a high transport critical current density. *Supercond. Sci. Technol.* **23,** 075005 (2010).
14. Gao, Z. *et al.* Superconducting properties of granular $SmFeAsO_{1-x}F_x$ wires with $T_c = 52$ K prepared by the powder-in-tube method. *Supercond. Sci. Technol.* **21,** 112001 (2008).
15. Yamamoto, A. *et al.* Evidence for electromagnetic granularity in polycrystalline Sm1111 iron-pnictides with enhanced phase purity. *Supercond. Sci. Technol.* **24,** 045010 (2011).
16. Kametani, F. *et al.* Intergrain current flow in a randomly oriented polycrystalline $SmFeAsO_{0.84}$ oxypnictide. *Appl. Phys. Lett.* **95,** 142502 (2009).
17. Qi, Y. *et al.* Transport critical currents in the iron pnictide superconducting wires prepared by the *ex situ* PIT method. *Supercond. Sci. Technol.* **23,** 055009 (2010).
18. Fujioka, M. *et al.* Effective *ex-situ* fabrication of F-doped SmFeAsO wire for high transport critical current density. *Appl. Phys. Express* **4,** 063102 (2011).
19. Sun, D., Liu, Y. & Lin, C. Comparative study of upper critical field H_{c2} and second magnetization peak H_{sp} in hole- and electron-doped $BaFe_2As_2$ superconductor. *Phys. Rev. B* **80,** 144515 (2009).
20. Wang, X-L. *et al.* Very strong intrinsic flux pinning and vortex avalanches in $(Ba,K)Fe_2As_2$ superconducting single crystals. *Phys. Rev. B* **82,** 024525 (2010).
21. Yang, H., Luo, H., Wang, Z. & Wen, H-H. Fishtail effect and the vortex phase diagram of single crystal $Ba_{0.6}K_{0.4}Fe_2As_2$. *Appl. Phys. Lett.* **93,** 142506 (2008).
22. Scanlan, R. M., Malozemoff, A. P. & Larbalestier, D. C. Superconducting materials for large scale applications. *Proc. IEEE* **92,** 1639–1654 (2004).
23. Braccini, V. *et al.* High-field superconductivity in alloyed MgB_2 thin films. *Phys. Rev. B* **71,** 12504 (2005).
24. Ozaki, T. *et al.* Fabrication of binary FeSe superconducting wires by novel diffusion process. *J. Appl. Phys.* (in the press); preprint at http://arxiv.org/abs/1103.3602(2011).
25. Togano, K., Matsumoto, A. & Kumakura, H. Critical properties of a dense polycrystalline $(Ba,K)Fe_2As_2$ superconductor prepared by a combined process of melting and deformation. *Supercond. Sci. Technol.* **23,** 045009 (2010).
26. Wang, C. *et al.* Enhanced critical current properties in $Ba_{0.6}K_{0.4+x}Fe_2As_2$ superconductor by overdoping of potassium. *Appl. Phys. Lett.* **98,** 042508 (2011).
27. Durrell, J. *et al.* Critical current of $YBa_2Cu_3O_{7-\delta}$ low-angle grain boundaries. *Phys. Rev. Lett.* **90,** 247006 (2003).
28. Song, X., Daniels, G., Feldmann, D. M., Gurevich, A. & Larbalestier, D. Electromagnetic, atomic structure and chemistry changes induced by Ca-doping of low-angle $YBa_2Cu_3O_{7-\delta}$ grain boundaries. *Nature Mater.* **4,** 470–475 (2005).

Acknowledgements

W. Starch, M. Hannion, M. Santos and V. Griffin provided technical support. This work is supported by NSF DMR-1006584, by the National High Magnetic Field Laboratory, which is supported by the National Science Foundation under NSF/DMR-0084173, and by the State of Florida.

Author contributions

J.D.W. synthesized all samples, carried out X-ray diffraction, electromagnetic and SEM characterization, and prepared the manuscript. C.T. carried out the high-field resistivity measurements and prepared the manuscript. J.J. carried out electromagnetic characterization and helped design the experiments. F.K. carried out TEM measurements. A.A.P. carried out magneto-optical imaging. D.C.L. and E.E.H. directed the research and contributed to manuscript preparation. All authors discussed the results and implications and commented on the manuscript.

Additional information

The authors declare no competing financial interests. Supplementary information accompanies this paper on www.nature.com/naturematerials. Reprints and permissions information is available online at www.nature.com/reprints. Correspondence and requests for materials should be addressed to E.E.H.